A method for spatial deconvolution of spectra

F. Courbin
Universidad Católica de Chile,
Departamento de Astronomia y Astrofisica, Casilla 306, Santiago 22, Chile;
Institut d'Astrophysique et de Géophysique de Liège, Avenue de Cointe 5, B-4000 Liège, Belgium;
fcourbin@astro.puc.cl

P. Magain[1], M. Kirkove[2], S. Sohy
Institut d'Astrophysique et de Géophysique de Liège, Avenue de Cointe 5, B-4000 Liège, Belgium;
Pierre.Magain@ulg.ac.be, Murielle.Kirkove@ulg.ac.be, Sandrine.Sohy@ulg.ac.be

ABSTRACT

A method for spatial deconvolution of spectra is presented. It follows the same fundamental principles as the "MCS image deconvolution algorithm" (Magain, Courbin, Sohy, 1998) and uses information contained in the spectrum of a reference Point Spread Function (PSF) to spatially deconvolve spectra of very blended sources. An improved resolution rather than an infinite one is aimed at, overcoming the well known problem of "deconvolution artefacts". As in the MCS algorithm, the data are decomposed into a sum of analytical point sources and a numerically deconvolved background, so that the spectrum of extended sources in the immediate vicinity of bright point sources may be accurately extracted and sharpened. The algorithm has been tested on simulated data including seeing variation as a function of wavelength and atmospheric refraction. It is shown that the spectra of severely blended point sources can be resolved while fully preserving the spectrophotometric properties of the data. Extended objects "hidden" by bright point sources (up to 4-5 magnitudes brighter) can be accurately recovered as well, provided the data have a sufficiently high total signal-to-noise ratio (200-300 per spectral resolution element). Such spectra are relatively easy to obtain, even down to faint magnitudes, within a few hours of integration time with 10m class telescopes.

Subject headings: Data processing: spectroscopy - deconvolution

[1]Also Maître de Recherches au FNRS (Belgium)

[2]Aspirante au FNRS (Belgium)

1. Background and motivation

Tremendous efforts have been devoted to the development of numerical methods aimed at improving the spatial resolution of astronomical images. However, the techniques proposed so far and most commonly used (e.g., Richardson, 1972, Lucy, 1974, Skilling & Bryan, 1984), tend to produce the so-called "deconvolution artefacts" (oscillations in the vicinity of high spatial frequency structures) and to alter the photometric and astrometric properties of the original data. Recently, Magain, Courbin & Sohy (1998; hereafter MCS) proposed and implemented a new deconvolution algorithm which overcomes such drawbacks. Its success is mainly the consequence of a deliberate choice to achieve an *improved* resolution rather than an infinite one, hence avoiding to retrieve spatial frequencies forbidden by the sampling theorem. Many successful applications of the algorithm have been carried out in the framework of an intensive effort to obtain detailed light/mass maps for lensing galaxies (e.g., Courbin et al. 1997, 1998, Burud et al. 1998a,b). These results, when compared with more recent Hubble Space Telescope (HST) images, demonstrate the efficiency of the method to produce reliable high resolution images.

Undoubtedly, high spatial resolution plays a key role in most of the major advances made in observational astrophysics. This is true not only in imaging, but also in spectroscopy. We present in this paper a spectroscopic version of the MCS algorithm and we demonstrate from realistic simulations that flux calibrated spectra of severely blended point sources can be accurately recovered. We also show how the algorithm can be used to decontaminate the spectrum of extended objects from light pollution by very nearby, eventually bright, point sources.

2. Spatial deconvolution of spectra

MCS have shown that sampled images should not be deconvolved with the observed Point Spread Function (PSF), but with a narrower function, chosen so that the final deconvolved image can be properly sampled, whatever sampling step is adopted to represent it. For this purpose, one can *choose* the final PSF $\mathcal{R}(\vec{x})$ of the deconvolved image and *compute* the PSF $\mathcal{S}(\vec{x})$ which should be used to perform the deconvolution instead of the *observed* PSF $\mathcal{T}(\vec{x})$. The profile $\mathcal{S}(\vec{x})$ may be obtained by inverting the equation (see Sect. 3.):

$$\mathcal{T}(\vec{x}) = \mathcal{S}(\vec{x}) * \mathcal{R}(\vec{x}), \tag{1}$$

where the symbol "$*$" stands for the convolution. Equation (1) should always be considered together with the important constraint that all three profiles must be properly sampled.

A straightforward consequence of *choosing* the shape of the PSF $\mathcal{R}(\vec{x})$ is that it is, indeed, exactly known. Such *prior knowledge* can be used to decompose the data (image or spectrum) into a sum of point sources with known analytical spatial profile, and a deconvolved numerical

background. This decomposition was successfully used in the MCS image deconvolution algorithm. We apply the same fundamental rule to construct an algorithm for the spatial deconvolution of spectra.

2.1. Constructing the algorithm

A 2-D spectrum can be described as M spectral resolution elements (e.g., M lines), composed of N spatial resolution elements (e.g., N columns). Each spectral resolution element of the spectrum can be approximated as a quasi-monochromatic 1-D image (see Appendix) that we decompose as in the MCS image deconvolution algorithm. The pixel intensities $\mathcal{F}(\vec{x})$ of such a 1-D image may then be written as

$$\mathcal{F}(\vec{x}) = \mathcal{H}(\vec{x}) + \sum_{k=1}^{N_\star} a_k \mathcal{R}(\vec{x} - \vec{c_k}), \tag{2}$$

which is the sum of a 1-D numerical deconvolved background $\mathcal{H}(\vec{x})$ and of $N_\star$ profiles $\mathcal{R}(\vec{x})$ with intensities a_k and centers c_k. The profile $\mathcal{R}(\vec{x})$ is chosen to be Gaussian, with fixed width (i.e., resolution) all along the spectral direction. The final deconvolved spectrum is therefore corrected for seeing variations with wavelength. Moreover, the spectra may suffer from slit misalignment with respect to the physical dimensions of the detector and from atmospheric refraction. As a consequence, the position of a given point source on the detector is wavelength dependent. The deconvolved (and decomposed) 2-D spectrum which matches the data at best, may therefore be obtained by minimizing the function

$$\mathcal{C}_{\chi^2} = \sum_{j=1}^{M} \sum_{i=1}^{N} \frac{1}{\sigma_{i,j}^2} \left[\mathcal{S}_j(\vec{x}) * \left(\mathcal{H}_j(\vec{x}) + \sum_{k=1}^{N_*} a_{k,j}\, \mathcal{R}(\vec{x} - \vec{c}_{k,j}) \right) - \mathcal{D}_j(\vec{x}) \right]_i^2, \tag{3}$$

where $\mathcal{D}_j(\vec{x})$ is the j^{th} spectral element of the data spectrum, $\mathcal{S}_j(\vec{x})$ is the j^{th} spectral element of the (narrower) PSF. Note that the width of the profile $\mathcal{S}(\vec{x})$ may vary with wavelength, as does the observed profile $\mathcal{T}(\vec{x})$, in order to ensure that $\mathcal{R}(\vec{x})$ does not. The sum over i is the summation of the N pixel values along the spatial direction of the M spectral resolution elements.

Importantly, the deconvolution has to be performed under the constraint that the deconvolved background $\mathcal{H}(\vec{x})$ is smooth on the length scale of the final resolution (represented by the profile $\mathcal{R}(\vec{x})$). This is efficiently done by minimizing

$$\mathcal{L}_1 = \sum_{j=1}^{M} \sum_{i=1}^{N} [\mathcal{H}_j(\vec{x}) - \mathcal{R}(\vec{x}) * \mathcal{H}_j(\vec{x})]_i^2 \tag{4}$$

where the notations and indices are the same as in equation (3). This smoothing applies in the spatial direction only and independently for each spectral resolution element.

In spectroscopy, one may take advantage of an additional prior knowledge available: the fact that the position of a given point source at a given wavelength is highly correlated with its position in the neighbouring spectral resolution elements. We introduce this prior knowledge as a second constraint:

$$\mathcal{L}_2 = \sum_{j=1}^{M} \left[c_j - \sum_{j'=-W/2}^{W/2} g_{j'} c_{j+j'} \right]^2 \tag{5}$$

where the function g has a Gaussian shape, for simplicity. It is defined over a box of W pixels centered on the j^{th} spectral resolution element. Its Full Width at Half Maximum (FWHM) $w_g = 2\sqrt{\frac{\ln 2}{b_g}}$ defines the typical scale length where the correlation applies. The function is normalized to a total flux of one and is simply written as

$$g_j = \frac{1}{G} e^{-b_g \cdot j^2}, \tag{6}$$

$$G = \sum_{j=-W/2}^{W/2} g_j$$

The final algorithm we propose for the spatial deconvolution of spectra therefore involves the minimization of the function

$$\mathcal{C} = \lambda \mathcal{C}_{\chi^2} + \mathcal{L}_1 + \mu \mathcal{L}_2 \tag{7}$$

The Lagrange multipliers λ and μ should be chosen so that the deconvolved spectrum matches the data correctly, in the χ^2, once it is re-convolved with the PSF $\mathcal{S}(\vec{x})$. This is described for image deconvolution in Courbin et al. (1997, 1998) and Burud et al. (1998a,b) and in the following section for the specific case of spectra.

3. Simulations

The algorithm is tested on two different types of simulated data. The first simulation involves blends of point sources only, while the second one also considers extended sources, hence illustrating the capability of the algorithm to unveil faint extended objects hidden by much

brighter ones. Both simulations include the effects of slit misalignment, seeing variation as a function of wavelength, as well as exaggerated atmospheric refraction. Gaussian photon noise and readout noise are also added to the data. A typical signal-to-noise ratio for the data is 200-300 per spectral resolution element. The deconvolutions are performed as in imaging and the optimal choice of the different Lagrange multipliers to be used is guided by the visual inspection of the residual maps (RM). The RM is the difference between the raw data and the deconvolved image re-convolved by the PSF $\mathcal{S}(\vec{x})$, in units of the noise. An accurate deconvolution should therefore leave a flat RM with a mean value of 1.

3.1. Blended point sources

The two point sources included in the simulations are separated by two pixels and are observed with a resolution of 4 pixels FWHM. The deconvolved spectra have a resolution of 2 pixels FWHM. Figure 1 compares the spatial profiles of the simulated data before and after deconvolution. In all simulations, the PSF used is *not assumed to be perfectly known*. It is determined from the spectrum of a simulated star by applying the PSF construction algorithm described in Section 4.

We first test the algorithm on a blend of two very different objects, with extreme and opposite colors. For example, Figures 2 and 3 consider the spectrum of a quasar contaminated by that of a star of similar or fainter luminosity (from 0. to 1.8 mag fainter depending on wavelength). Figure 2 shows the result of the deconvolution as well as the RM which reflects the good agreement between the data and the deconvolved spectrum all along the wavelength range considered. Figure 3 displays the 1-D spectra obtained by integrating the light of the 2-D spectra along the spatial direction, together with the flux ratio between the deconvolved spectra and the spectra used to build the simulated data (insets). The latter clearly demonstrates that (1) the simulated and recovered spectra agree very well within the noise and (2) there is no mutual light contamination between the spectra.

A second test involves a blend of point sources with identical spectra but different luminosities, e.g., the images of a lensed quasar. Our simulation consist of two quasar images with magnification ratio of 1.8 mag. As in our first example, the separation between the sources is 2 pixels and the spectra have a spatial resolution of 4 pixels FWHM. The 1-D deconvolved spectra are displayed in Figure 4, confirming the results obtained with our first simulation. Figure 4 also illustrates the effect of the correlation introduced in equation 5 on the position of the sources as a function of wavelength. While the deconvolved spectra on the left panels were obtained without introducing any correlation ($\mu = 0$ in equation 7), the ones on the right panels were obtained by choosing the μ parameter leading to the best possible RM. Choosing a too small μ multiplier leads to over-fitting of the data and to a "noisy" deconvolved spectrum, while a larger μ leads to under-fitting.

3.2. Extended sources

The simulations presented in the previous section show that the algorithm is efficient in deconvolving/extracting the individual spectra of very blended point sources and that their relative flux distribution is not modified by the deconvolution process. We now show how the algorithm can also be used to extract the spectrum of extended faint objects hidden by (eventually much brighter) point sources.

Figure 5 presents the results of such a simulation. The spectra of two quasar images are generated, with a separation of 6 pixels. The spatial resolution is 4 pixels FWHM and the signal-to-noise ratio of the brightest spectrum is about 200-300 per spectral resolution element, depending on wavelength. The flux ratio between the QSO images is 3 (1.2 magnitudes). The spectrum of the – extended – lensing galaxy is also incorporated in the simulated data. It is situated only 2 pixels away from the centroid of the faintest QSO image and is about 3 to 5 magnitudes fainter than the QSO images (depending on wavelength) and therefore completely invisible in the raw data (see panel (a) of Figure 5). Panel (b) shows the result of the deconvolution, panel (c) displays the 2-D deconvolved spectrum of the lensing galaxy alone. This spectrum is our best result among a number of deconvolutions using different smoothness intensities and different correlation factors on the center of the point sources (λ and μ in equation 7). The RM, as defined at the beginning of this section is displayed in panel (e) and does not show any significant structure, as expected for an appropriate choice of λ and μ. Figure 6 confirms the good results obtained in Figure 5. The 1-D spectra of the 2 QSO images as well as the spectrum of the very faint lensing galaxy are in very good agreement with the input spectra, in spite of the blending and high luminosity contrast. The emission line in the spectrum of the lensing galaxy is well recovered and its (spectral) position is retrieved with an accuracy of 0.1 pixel.

4. Generating the PSF

Deconvolving spectra requires a good knowledge of the instrumental PSF all along the wavelength range available. This condition is fulfilled as soon as the spectrum of a star or any other point source is recorded together with the spectrum of scientific interest. The construction of the PSF is carried out as with the image deconvolution algorithm, i.e., the PSF $\mathcal{S}(\vec{x})$ is modeled as the sum of a Moffat profile and of a numerical image containing all small residual differences between the Moffat and the observed PSF. The analytical one dimensional spatial profile at wavelength j is simply written as:

$$\mathcal{M}_j(\vec{x}) = a_j \left[1 + b_j \left(\vec{x} - c_j\right)^2\right]^{-\beta}, \tag{8}$$

where a_j is the intensity of the profile, b_j defines its width, c_j is its center along the spatial direction and β characterizes the wings of the profile. $\mathcal{M}(\vec{x})$ must have the resolution of the PSF

$\mathcal{S}(\vec{x})$ needed for the deconvolution process and is obtained by minimizing the χ^2 between the observed PSF $\mathcal{T}(\vec{x})$ and $\mathcal{M}(\vec{x}) * \mathcal{R}(\vec{x})$. As in the MCS deconvolution, $\mathcal{R}(\vec{x})$ is the *adopted* shape of the PSF after deconvolution. The χ^2 can be written as follow:

$$\chi^2_{\mathcal{M}} = \sum_{j=1}^{M}\sum_{i=1}^{N} \frac{1}{\sigma^2_{i,j}} \left[\mathcal{R}(\vec{x}) * \mathcal{M}_j(\vec{x} - \vec{c_j}) - \mathcal{T}_j(\vec{x} - \vec{c_j})\right]^2_i \tag{9}$$

where the i and j indices are respectively running along the spatial and spectral directions. As for the deconvolution, it is highly desirable to use any prior knowledge available on the shape and position of the PSF spectrum. The center c_j of the spectrum at wavelength j is highly correlated to the position at neighbouring wavelength. The same constraint can be applied to the shape (b and β in equation 8) of the Moffat profile. Such constraints are taken into account by minimizing equation (9) together with the three constraints:

$$\mathcal{L}_1 = \sum_{j=1,}^{M} \left[c_j - \frac{1}{G} \sum_{j'=-W/2}^{W/2} g_{j'} c_{j+j'} \right]^2 \tag{10}$$

$$\mathcal{L}_2 = \sum_{j=1,}^{M} \left[b_j - \frac{1}{G} \sum_{j'=-W/2}^{W/2} g_{j'} b_{j+j'} \right]^2 \tag{11}$$

$$\mathcal{L}_3 = \sum_{j=1,}^{M} \left[\beta_j - \frac{1}{G} \sum_{j'=-W/2}^{W/2} g_{j'} \beta_{j+j'} \right]^2 \tag{12}$$

where the function g is the same as in equations (5) and (6). Constructing the analytical Moffat component of the PSF can therefore be done by minimizing the function:

$$\mathcal{C}_1 = \chi^2_{\mathcal{M}} + \mu_1\mathcal{L}_1 + \mu_2\mathcal{L}_2 + \mu_3\mathcal{L}_3 \tag{13}$$

The strengths of the correlations introduced on the shape and position of the Moffat profile are modified by the three Lagrange multipliers μ_1, μ_2, μ_3. While their choice obviously influences the quality of the fit, it is not a critical parameter. Indeed, a PSF is never a perfect Moffat profile and a numerical residual image has to be added to the analytical component of the PSF. Thus, the parameters μ_1, μ_2 and μ_3 have to be chosen so that $\mathcal{M}(\vec{x})$ matches at best the PSF, but an additional numerical component is *mandatory* to build $\mathcal{S}(\vec{x})$ with the accuracy required for the deconvolution algorithm to work properly. This numerical image $\mathcal{F}(\vec{x})$ must not contain any structure of spatial frequency above the highest frequency contained in $\mathcal{R}(\vec{x})$. It is therefore constructed by minimizing:

$$\begin{aligned} \mathcal{C}_2 &= \sum_{j=1}^{M}\sum_{i=1}^{N} \frac{\lambda}{\sigma_{i,j}^2} \left[\mathcal{R}(\vec{x}) * \mathcal{F}_j(\vec{x}) - \mathcal{K}_j(\vec{x})\right]_i^2 \\ &+ \sum_{j=1}^{M}\sum_{i=1}^{N} \left[\mathcal{F}_j(\vec{x}) - \mathcal{R}(\vec{x}) * \mathcal{F}_j(\vec{x})\right]_i^2 , \end{aligned} \tag{14}$$

where,

$$\mathcal{K}(\vec{x}) = \mathcal{T}(\vec{x}) - [\mathcal{R}(\vec{x}) * \mathcal{M}(\vec{x})] \tag{15}$$

is the numerical component of the PSF.

The Lagrange parameter λ is chosen so that $\mathcal{F}(\vec{x}) * \mathcal{R}(\vec{x})$ matches at best $\mathcal{K}(\vec{x})$ in the sense of a χ^2 and the final PSF is simply the sum of $\mathcal{M}(\vec{x})$ and $\mathcal{F}(\vec{x})$.

The result of the process is a PSF $\mathcal{S}(\vec{x})$ which incorporates seeing variations as a function of wavelength and takes into account atmospheric refraction. Using such a PSF for the deconvolution of spectra affected by the same atmospheric refraction therefore leads to a deconvolved spectrum corrected both for seeing variation and for atmospheric refraction.

One may first think that obtaining the spectrum of a reference star is a serious limitation to the technique. However, while for some applications (e.g., multiple QSOs) long slit spectroscopy may be difficult since a suitable PSF star well aligned with the different objects of interest might not be available, observing with a Multi Object Spectrograph (MOS) will in most cases not only allow to observe the blended objects, but also to obtain simultaneously the spectra of one or more PSFs. Observing several PSF stars has the further advantage of allowing substantial improvement of the spatial sampling. Higher spatial resolution can then be achieved as well as a more accurate point source/background separation. In any case, either in long slit spectroscopy or MOS, particular care should be paid to the centering of objects and PSFs on the slit(s). The slit edges clip the PSF's wings. Although our deconvolution procedure can handle this, clipping has to be similar in the object spectrum and in the PSF spectrum. Observing with wide slits will minimize the effect of centering errors and PSF clipping.

5. Limitations: signal-to-noise and sampling

To any algorithm there are limitations. The present one is not an exception to the rule. Also, it should be understood that while improvement of the data is aimed at, the algorithm can not extract non-existing information.

Our simulations show that high S/N data are usually required to achieve accurate point-source/background separation, especially when dealing with strong blends. In the most extreme case of two objects exactly superposed, e.g., a QSO and its host galaxy, the quality of the decomposition also depends on the physical size of the extended object projected on the plane of the sky, as compared with the seeing value. As clearly there is no way to separate two or more PSFs located exactly at the same position, the main limitation in such a case remains the seeing of the observations.

In addition to the seeing, the spatial sampling of the data also influences the results. On 4m class telescopes pixel sizes tend to be large in order to beat readout noise and to observe faint objects. A common pixel size is $0.25''$or more, which often leads to poor or even critical sampling, in the case of near-IR spectrographs or space instruments. As a consequence, the gain in spatial resolution is often limited to less than a factor 2 for data taken with present day spectrographs. However, the situation is improving, as 8m class telescopes have much smaller pixel sizes, of the order of $0.1''$. In addition, our algorithm can make use of an oversampled PSF (in the spatial direction) which is obtained from the spectra of several PSF stars. Such observations are possible in MOS mode. The spatial information needed to restore the PSF spectrum on a grid of pixels smaller than in the original data is then available, as the PSF spectra are not all centered in the same way, relative to the central pixel of each slitlet. According to the sampling theorem, the gain in resolution in only limited by the sampling *in the deconvolved spectrum*, not by the sampling of the original data. This sampling can in principle be as small as the user wishes, but we restrict ourselves to a factor two gain. The number of PSF stars to be observed simultaneously to improve further the sampling would be too large. This still allows substantial improvement of the spatial resolution, even for critically sampled data. Note finally, that even if the use of an oversampled PSF allows one to deconvolve critically sampled spectra, better sampling (FWHM $\sim$ 5-6 pixels) leads, as one should expect, to much more reliable results, in particular in view of accurate background/point source separation.

6. Conclusions

We have described a new method for the spatial deconvolution of spectra which can be used not only to de-blend point sources, but also to decompose spectra into a sum of point sources and extended sources. We have shown from realistic simulations that the relative flux distribution in such deconvolved spectra is very well recovered, hence making it possible to perform accurate spectrophotometric measurements of very blended objects. In our simulations, we resolve and extract the individual spectra of sources separated by only 2 pixels, under seeing conditions of 4 pixels FWHM. For modern spectrographs mounted on 8-10m class telescopes, this is equivalent to sources separated by 0.2-0.3$''$under 0.4-0.6$''$seeing conditions. The signal-to-noise required for the method to work efficiently is of the order of 200, which is presently easy to reach in a few hours integration time, even down to magnitudes of the order of 21-22.

Clearly, the new extension of the MCS image deconvolution algorithm has a wide field of applications (see Courbin et al. 1999 for more details on how to use the algorithm in practise). The most original and promising applications may consist in spectroscopic studies involving extended objects hidden by – often brighter – point sources. Our simulations show an example of application to gravitationally lensed quasars, where the redshift of a very faint lensing galaxy can be measured, hence making it possible to estimate H_0 from multiply imaged QSOs with known time delays. A similarly interesting application will be to take full advantage of the ability of the algorithm to decompose spectra, in order to carry out the first systematic spectroscopic study of quasar host galaxies. With current instrumentation mounted on 8-10m class telescopes, sufficiently high signal-to-noise spectra can be obtained for low redshift quasars in order to derive precise rotation curves of their host galaxy, provided the spectrum of the bright QSO nucleus can be removed accurately. The present spectra deconvolution algorithm is very well suited for such a purpose and may therefore allow significant progress towards the measurement of the mass of the central black hole in QSO host galaxies.

APPENDIX

We assume that the spatial deconvolution of spectra simplifies to a number of independent deconvolutions of quasi-monochromatic 1-D images. This assumption makes sense if, (*i*) the PSF is stable in the spatial direction (*ii*) it varies slowly with wavelength, i.e., it does not show any significant changes in the spectral direction on a length scale comparable to the seeing disk at a given wavelength and, (*iii*) the PSF is separable.

Conditions (*i*) and (*ii*) are usually fulfilled provided PSFs stars can be found close to the objet to deconvolve and provided very low spectral resolution is not aimed at. Condition (*iii*) might be more difficult to fulfill exactly. Using the same notations as in the main body of the paper, but this time in 2 dimensions, we note $\mathcal{S}(x, y)$ the (narrower) PSF at pixel (x, y), where x is in the spatial direction and y is in the spectral direction. $\mathcal{S}$ is separable if it can be written as

$$\mathcal{S}(x, y) \quad = \quad \mathcal{H}_y(x)\mathcal{K}(y), \tag{16}$$

where $\mathcal{H}_y(x)$ and $\mathcal{K}(y)$ are two 1-D spatial distributions. The index y refers to possible variations of the PSF $\mathcal{H}_y(x)$ with wavelength. In other words, $\mathcal{S}(x, y)$ is not necessarily symmetric about its center but, if elongated, must have its major axis parallel (or perpendicular) to the slit. In practice, this means that the algorithm may not be fully applicable if significant tracking errors affect the data.

In the following we will assume that the instrument used to take the data has a decent optical quality, operates at relatively high spectral resolution and has a reliable tracking system. We can then write the (noise free) intensity of a data pixel $\mathcal{D}(x, y)$ as

$$\mathcal{D}(x,y) = \mathcal{S}_y(x,y) * \mathcal{F}(x,y) \tag{17}$$

where $\mathcal{F}(x,y)$ is the signal of scientific interest. Moderately high spectral resolution ensures us that $\mathcal{S}_y(x,y)$ does not vary too fast with wavelength. We can therefore assume that it is constant over a spatial area approximately equal to the seeing disk. We can now consider only one 1-D spectral resolution element y so that $\mathcal{S}_y(x,y)$ can be simplified to $\mathcal{S}(x,y)$. Blurring by the spectral PSF of the spectrograph $\mathcal{W}(y)$ leads to

$$\mathcal{D}(x,y) = \int \left[\mathcal{S} * \mathcal{F}\right](x,y')\mathcal{W}(y-y')\,dy' \tag{18}$$

or more explicitly,

$$\mathcal{D}(x,y) = \int\int\int \mathcal{S}(x-x",y'-y")\mathcal{F}(x",y")\,dx"\,dy"\mathcal{W}(y-y')\,dy' \tag{19}$$

Now, we can write,

$$\mathcal{L}(x-x",y-y") = \int \mathcal{S}(x-x",y'-y")\mathcal{W}(y-y')\,dy'$$

to obtain,

$$\mathcal{D}(x,y) = \mathcal{L}(x,y) * \mathcal{F}(x,y) \tag{20}$$

Therefore, if $\mathcal{S}(x,y)$ is separable, $\mathcal{L}(x,y)$ is also separable, so that we can finally write $\mathcal{D}(x,y)$ as the convolution of a spectrum with a 1-D profile in the spatial direction:

$$\mathcal{D}(x,y) \quad = \quad \mathcal{H}(x) * [\mathcal{K}(y) * \mathcal{F}(x,y)] \tag{21}$$

with

$$\mathcal{L}(x,y) = \mathcal{H}(x)\mathcal{K}(y) \tag{22}$$

The function $\mathcal{K}(y) * \mathcal{F}(x,y)$ is the spectrum of scientific interest, and $\mathcal{H}(x)$ has here the same role as the 1-D PSF $\mathcal{S}(x)$ used in the algorithm.

F. Courbin acknowledges financial support from Chilean grant FONDECYT/3990024. M. Kirkove and S. Sohy are supported by contracts ARC 94/99-178 "Action de Recherche Concertée de la Communauté Française (Belgium)" and "Pôle d'Attraction Interuniversitaire" P4/05 (SSTC Belgium). We also thank the European Southern Observatory for additional support.

REFERENCES

Burud, I., Courbin, F., Lidman, C., et al. 1998a, ApJ, 501, L5

Burud, I., Stabell, R., Magain, P., et al. 1998b, A&A, 339, 701

Courbin, F., Magain, P., Keeton, C.R., et al. 1997, A&A, 324, L1

Courbin, F., Lidman, C., Frye, B., et al. 1998, ApJ, 499, L119

Courbin, F., Magain, P., Sohy, S., Lidman, C., Meylan, G., 1999, ESO-Messenger, in preparation

Lucy, L. 1974, AJ, 79, 745

Magain, P., Courbin, F., & Sohy, S. 1998, ApJ, 494, 472

Richardson, W.H.J. 1972, J. Opt. Soc. Am., 62, 55

Skilling, J., & Bryan, R.K. 1984, MNRAS, 211, 111

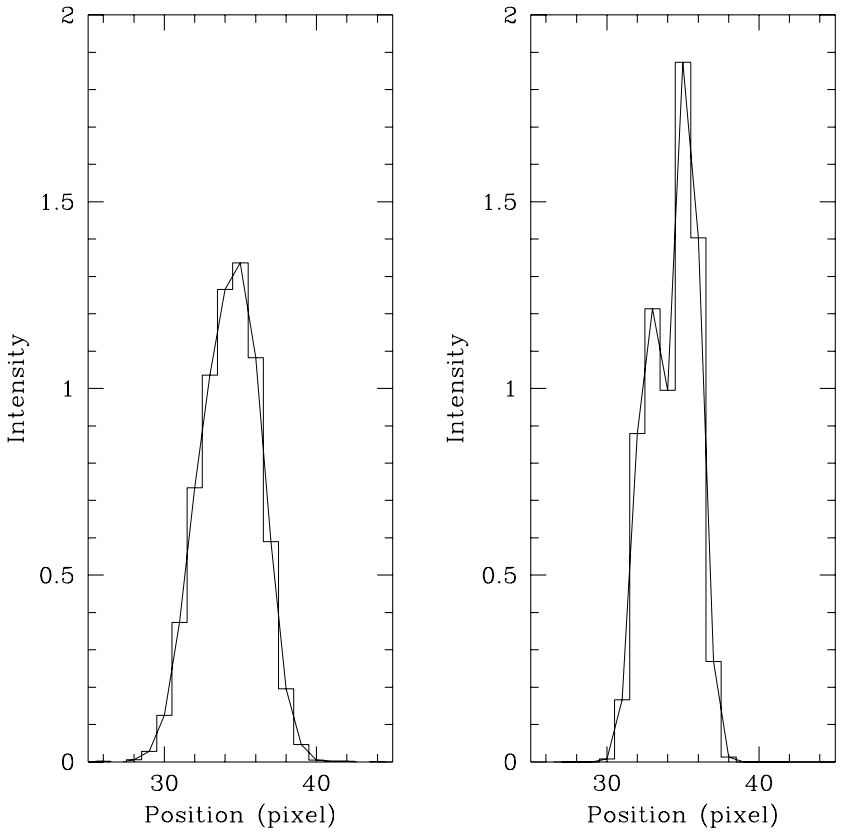

Fig. 1.— One-dimensional spatial profile of the simulated spectrum before (left) and after (right) deconvolution. The two point sources are perfectly recovered.

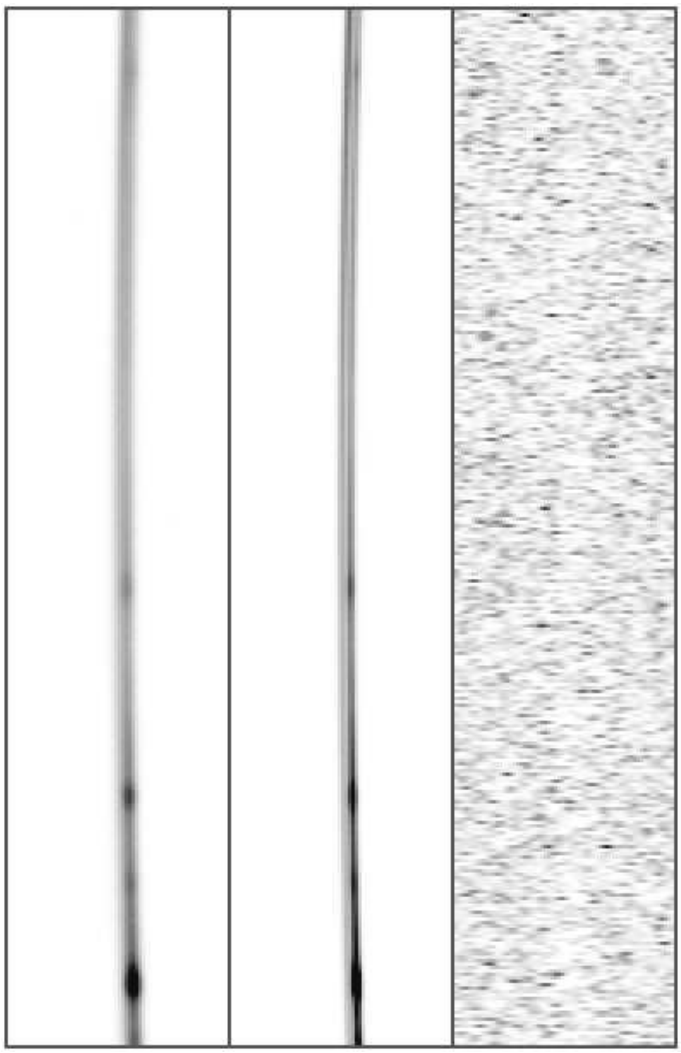

Fig. 2.— Left: Two-dimensional simulated spectrum of a blend of point sources separated by 2 pixels. The spatial resolution of the spectrum is 4 pixels FWHM and its curvature simulates strong atmospheric refraction. Middle: 2-D deconvolved version of the spectrum. Two spectra are now – almost – resolved. An object with a continuum-only spectrum can be seen on the left side of the spectrum while an emission line object dominates the total flux on the right side. Right: Residual map used as a quality check of the deconvolution. It is flat and equal to 1σ.

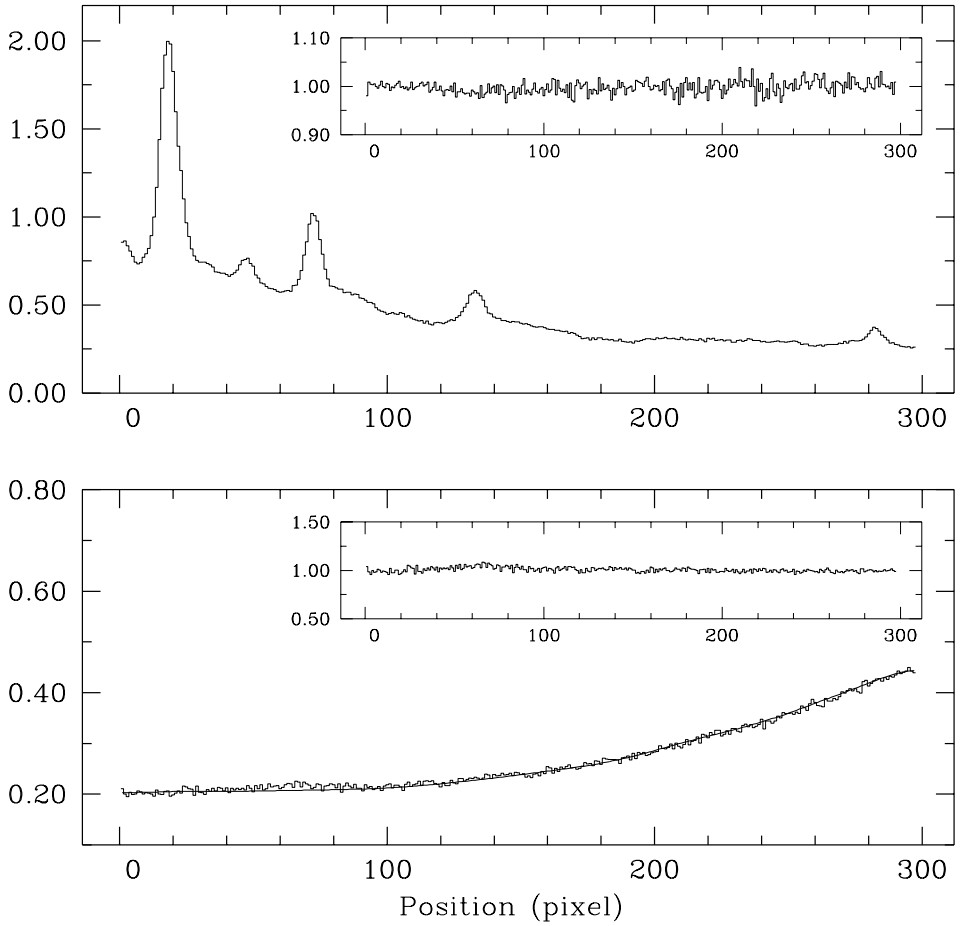

Fig. 3.— Top: deconvolved 1-D spectrum of one of the blended point source (a quasar). Bottom: deconvolved 1-D spectrum of the second point source with only a continuum. In both figures the inset displays the flux ratio between the known spectrum used build the simulated data and the deconvolved spectrum. The scale on the horizontal axis is arbitrary, in pixels.

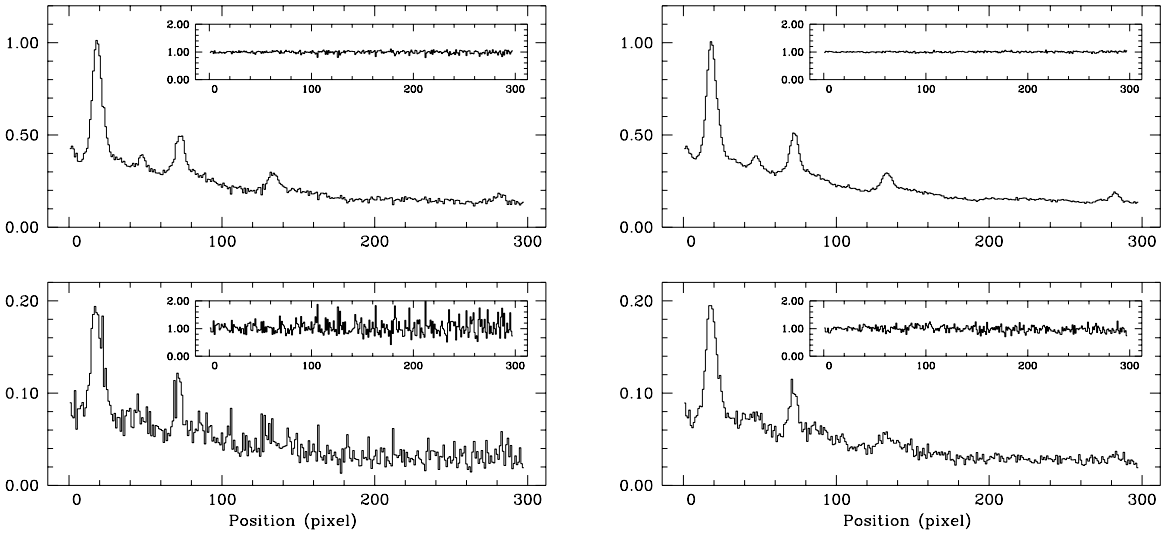

Fig. 4.— Left: 1-D deconvolved QSO spectra, where the inset is as in Figure 3. The deconvolution is performed with $\mu = 0$ (see equation 7). Right: As on the left panel but with the correct choice for μ (see section 3.1). Note how the signal-to-noise improves with an appropriate choice of the correlation parameter μ.

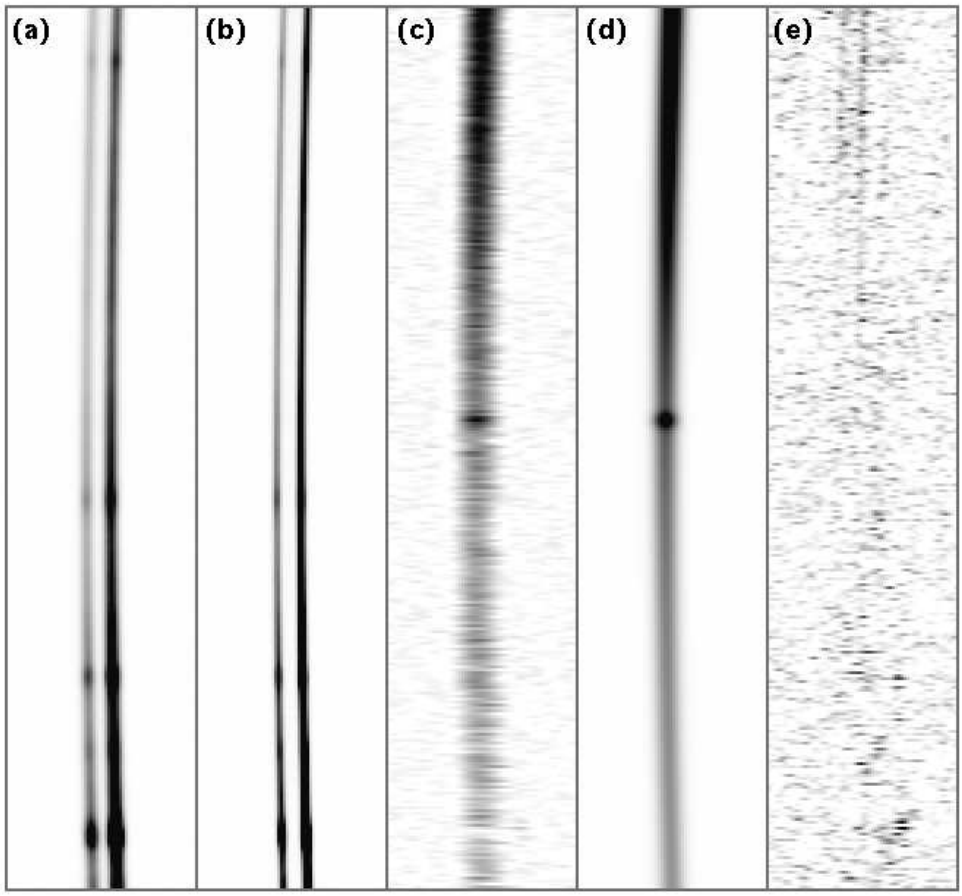

Fig. 5.— From left to right: (*a*) Simulated spectrum of a lensed quasar ($\sim 4000 - 8000$Å), (*b*) its deconvolution, (*c*) the deconvolved background (here, the lensing galaxy alone), (*d*) the galaxy used to construct the simulation, and (*e*) the residual image (data minus model) in units of the photon noise. The simulation includes the effects of seeing variation with wavelength and (exaggerated) atmospheric refraction.

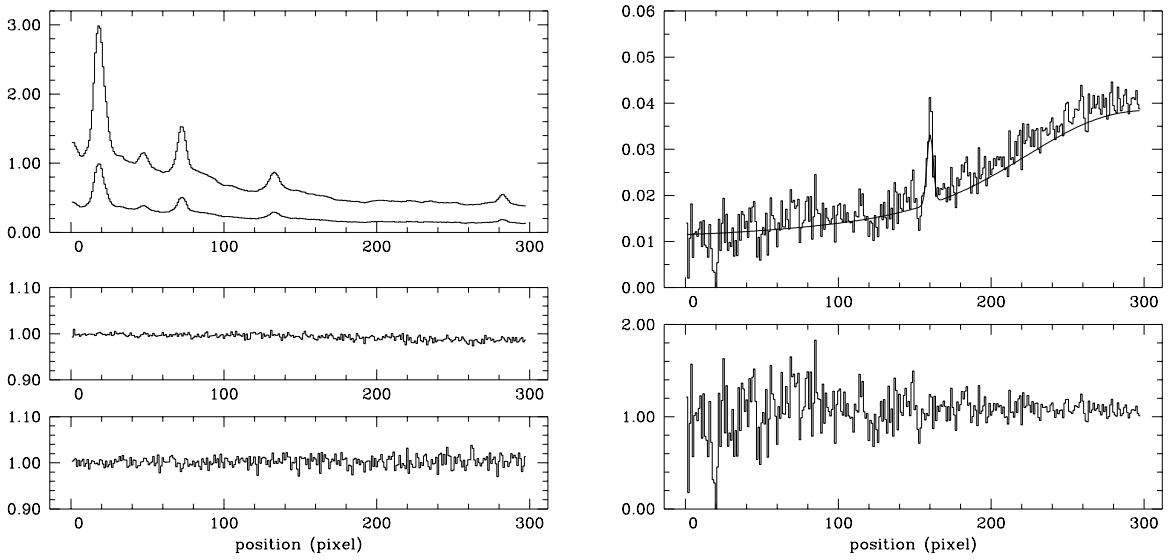

Fig. 6.— Left: The top panel shows the 1-D deconvolved spectra of the two simulated QSO images. In the middle and bottom panels are displayed the flux ratio between the two spectra and the original QSO spectrum used in the simulation. Right: the spectrum of the lensing galaxy alone (top) and its division by the input spectrum (bottom). The position of the emission line is retrieved with a accuracy of 0.1 pixel.